A Joint Design for Multi-band Heterogeneous Networks when Deploying Reconfigurable Intelligent Surface

Wenyu Jiang, Kaizhi Huang, Yajun Chen, Xiaoli Sun, Jie Yang, and Kai Zhao

***Abstract*—Reconfigurable intelligent surface (RIS) technique is effective to improve the capacity and coverage of various networks. However, the practical RIS has dissimilar responses to signals in different frequencies due to its structure. Therefore, directly applying existing schemes to multi-band heterogeneous networks leads to beam misalignment and performance degradation issues. This paper considers RIS-assisted multi-band heterogeneous networks where base stations (BSs) use different frequencies. We formulate the problem for maximizing the sum rate of all users (SR) in every frequency band, and aim to jointly design BSs precoding vectors and RIS parameters while taking user choices into account. Based on the closed-form relationship of phase shifts between frequencies, an iterative algorithm is proposed to solve the challenging non-convex problems. In particular, we use fractional programming to decouple the problem, and solve the subproblems with quadratic transform (QT) and genetic algorithm (GA). Simulation results show that the proposed scheme can significantly improve SR among all frequency bands, which could instruct the coexistence of multiple communication systems in future heterogeneous networks. What's more, results also prove that deploying RISs recklessly will result in a degradation of the network.**

***Index Terms*—Convex optimization, multi-band heterogeneous networks, practical model, reconfigure intelligent surface.**

I. Introduction

THE promotion and prevalence of 5G have greatly improved the quality of wireless cellular networks with their high speed and low latency. Even so, the exponential growth of cellular traffic brought by the increasing demand for portable intelligent equipment, mobile office etc., results in power consumption and mobility issues. Consequently, research community is already looking for a better vision for 6G technology due to the urgent need for higher system capacity and better edge coverage [1]. As a revolutionary enabling technology, reconfigurable intelligent surface (RIS) provides a new paradigm for wireless communication [2].

RIS contains a series of configurable electromagnetic internals, and is capable of precisely controlling parameters such as phase shifts and amplitude of the electromagnetic wave in a predefined manner [3]. RIS can effectively improve the performance of average rate [4] and coverage [5], by intervening and changing the environment of signal propagation. This characteristic generates significant interest in both academia and industry, and has been extended to millimeter waves (mmWave), physical layer security, device-to-device, and wireless powered systems [6]–[9], etc.

While people are excited about the benefits, many farsighted have raised their concerns. As RIS is gradually put into practice, existing ideal assumptions lead to serious issues in RIS deployment [10]. For example, the authors in [11] mention the management issues and believe that the addition of RIS may affect the operation status of other existing systems. The main problem lies in the working mechanism of RIS. Internal components of RIS adjust electromagnetic waves by changing the frequency-dependent reflecting coefficients. As an increment of the transmission environment, RIS will not only affect all links, but also have different effects on different frequencies [12], which may cause problems in existing systems.

In the multi-band heterogeneous networks which contains different systems with different frequencies, the RIS may not improve the performance but degrade intricate systems having different frequency bands. Moreover, in the foreseeable future, various communication technologies and frequency bands such as WiFi and cellular networks [13], telecommunications suppliers using different frequency bands [14] will be applied, and the drawback will be more evident.

There is no mutual influence between frequencies in traditional networks, and few research pays attention to this aspect. Facing multiple frequencies interweaving and coexisting in the electromagnetic environment, [15] and [16] consider a RIS aided OFDM system. These proposals reduce the estimation overhead by combining RIS elements, and obtain the maximum achievable rate by finding the optimal phase shifts and power allocation through an optimization algorithm. The authors in [17] studies the effect of RIS on OFDM signals under selective high-mobility Rician channels in UAV networks, and proposes estimation and interference canceling methods to obtain a better performance. In the multi-band cell-free network, Zhang uses multiple RISs to improve the sum of weighted rate of the whole network, hoping to replace the role of base station (BS) with RIS [18]. The optimal precoding and phase shifts are solved by developing an alternating optimization framework.

However, these studies only address the case where the RIS response to different frequencies is consistent, which will

Manuscript received April 15, 2022 revised June 23, 2022; approved for publication by Cunhua Pan, Guest Editor, September 12, 2022.

W. Jiang, K. Huang, Y. Chen, X. Sun, and J. Yang are with Information Engineering University, Zhengzhou, China, emails: jwy513@hotmail.com, huangkaizhi@tsinghua.org.cn, chenyajun_cool@126.com, lgdxsunxiaoli@sina.com, yj_csu@126.com.

K. Zhao is with Purple Mountain Laboratories Ringgold standard institution, Nanjing, Jiangsu, China, email: k_zhao@126.com

Y. Chen is the corresponding author.

Digital Object Identifier: 10.23919/JCN.2022.000047

1229-2370/22/$10.00 © 2022 KICS

hinder practical applications of RIS. [19] and [20] mention the frequency selective surface, which is more effective for dual-band due to material constraints, wherefore it has limited application in large networks. The authors in [21] construct the basic structure and model of the RIS for the first time, and derive the electromagnetic model of RIS. Subsequently, [22] proposes an equivalent model of RIS by means of equivalent impedance, which significantly reduces the model's complexity. [23] and [24] summarize and simulate the corresponding models respectively, showing the effectiveness of the model.

The authors in [25] consider deploying multiple RISs in multiple cells with different frequency bands to minimize the transmit power. The phase shifts of non-serving frequencies are approximately constant when the frequency gap is enormous. However, such a model cannot be used when the frequency gap is slight, which limits the capability of RIS. The phase shifts relationship between different frequencies are still unclear. The authors in [26] focus on the RIS-assisted OFDM system, and give approximate relationships for different frequencies for the first time. Based on the relationship, optimization problems are constructed and solved by the block coordinate descent method. Nevertheless, the approximate model is only established in the narrow bandwidth, and it is difficult to fit in some wideband networks.

Nevertheless, in the multi-band heterogeneous network, the frequency gap is closely related to actual deployed systems with various frequencies, resulting in lower accuracy of approximate relationships. At the same time, users in the multi-band heterogeneous network can choose BS according to signal strength, which has not been investigated in existing researches. In addition, when the RIS is deployed without a specific design in the multi-band heterogeneous network, how much performance degradation it will cause is still unclear.

To address aforementioned issues, we try to reverse the dilemma when deploying RIS in the multi-band heterogeneous network, and improve the performance of whole network. Our main contributions are as follows:

- We establish a model of generic multi-band heterogeneous networks, where multiple BSs serve multiple users at different frequency bands. The user can freely change the BS during the communication process according to the signal strength. The model can be extended to other multi-band networks such as OFDM, cell-free networks and networks with different techniques such as satellite and cellular networks.
- For multi-band heterogeneous networks, we formulate the problem aiming at maximizing the sum rate of users (SR) among all frequency bands. In addition, we derive a closed-form relationship of phase shifts between different frequency bands using the practical model for the first time to guide scheme designing. Through jointly designing BS precoding vectors and RIS phase shifts, the proposed scheme can improve the performance of the whole network.
- To address the non-convex problem, we decouple the main problem into several sub-problems using fractional programming (FP) based on Lagrangian dual reformulation at first. The sub-problems are solved with the aid of quadratic transform and alternating optimization algorithm. In particular, we transform variables from RIS capacitors to phase shifts to improve the accuracy, and introduce the genetic algorithm (GA) to reduce the cost of the traverse search. Finally, the iterative optimization algorithm is summarized, and the feasible sub-optimal solution is found.
- Simulation results show that the proposed scheme can effectively improve the SR. We further investigate the effects of different RIS element numbers, deployment locations, and frequency gaps to provide guidance for RIS deployment. In addition, it is worth noting that deploying RIS regardless of the consequences does result in a degradation of the performance, and even worse than the condition with no RIS.

The rest of the paper is organized as follows. The system model of the multi-band heterogeneous network and corresponding SR maximization problem formulation are discussed in Section II. In Section III, we proposed the joint optimization for BS precoding vectors and RIS phase shifts. Simulation results are provided in Section IV to validate the performance of the proposed scheme in multi-band heterogeneous network. Finally, we conclude the paper and future works in Section V.

Notations: Bold capital letters in the formula represent matrices, bold lowercase letters represent vectors, and normal lowercase letters represent constant values. $(\bullet)^T, (\bullet)^H, (\bullet)^{N*M}$ denote the transpose, conjugate-transpose operations and the dimension of the matrix, respectively. $\mathbb{C}$ and $\mathbb{R}^+$ denote the set of complex and positive real numbers, respectively. $Re()$ denotes the real part of a complex number. $|\mathbf{a}|$ denotes the norm of vector $\mathbf{a}$. $\mathcal{O}(\bullet)$ is the time computational complexity.

II. System Model

To establish a more realistic and generalizable model, we first describe the architecture and signal model of general multi-band heterogeneous networks in section II-A. Based on the practical structure, the equivalent circuit model of RIS is introduced in section II-B. Finally in section II-C, we formulate the problem of maximizing the SR in the network.

A. System Architecture and Signal Model

We consider a multi-band heterogeneous network as shown in Fig. 1. The network contains B different BSs with M antennas which provide the same kind of service to the user in different frequency bands. The BSs in the network can represent access points from different frequency bands (i.e., 1.8 GHz and 2 GHz), different telecommunications suppliers, or different communication technologies (i.e., cellular networks and WiFi). We assume that each BS is working in narrow-band and other frequencies are beyond the filter bandpass range.

We assume that each BS is working in narrow-band and other frequencies are beyond the filter bandpass range. Considering the actual situation like cellular networks with different telecommunications suppliers, the user equipment can receive multiple frequency bands such as 2.3 GHz and 2.5 GHz

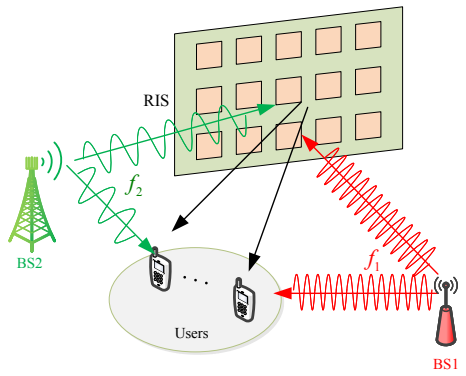

Fig. 1. The illustration of the proposed multi-band heterogeneous network.

around, and tends to select a BS with a higher quality of service (QoS).

In order to improve the rate of K single-antenna users among all frequency bands, a RIS with N elements is deployed near BSs. Let $\mathcal{B} = \{1, 2, \cdots, B\}$, $\mathcal{K} = \{1, 2, \cdots, K\}$ and $\mathcal{N} = \{1, 2, \cdots, N\}$ denote sets of BSs, users and elements of RIS, respectively.

At the beginning of the communication process, the acquisition of CSI is a critical step. Users broadcast the training pilots to all BSs. Under the assumption that BSs can obtain accurate CSI, BSs jointly design the precoding vectors and parameters of RIS elements in the downlink transmission process. After receiving the downlink signal, users judge the signal strength in each frequency band and automatically select the BS to access to. During the downlink transmission stage, each BS uses a particular frequency $f_s, s \in \mathcal{B}$ to transmit signals so that the signals do not interfere with each other. Let $\mathbf{s} = [s_{s,1}, s_{s,2}, \cdots s_{s,K}]^T \in \mathbb{C}^{K\times 1}$, where the $s_{s,k}$ demonstrates the signal from $s-th$ BS to the user K and has a normalized power.

Since there is no mutual influence at the signal level, the precoding vectors will be designed independently. The BS's precoding vectors $\mathbf{W} = [\mathbf{w}_{1,1}, \mathbf{w}_{1,2}, \cdots, \mathbf{w}_{B,K}]^T, \mathbf{w}_{s,k} \in \mathbb{C}^{M\times K}$ is used to encode the signal, and then the BS transmit symbol is denoted as $\mathbf{x}_s = \sum_{k=1}^{K} \mathbf{w}_{s,k} s_{s,k}$. Through the above assumptions, the received signal of the $k-th$ user can be expressed as:

$$\mathbf{y}_{s,k} = \mathbf{f}_{sU_k}^H \mathbf{w}_{s,k} s_{s,k} + \sum_{i=1, i\neq k}^{K} \mathbf{f}_{sU_k}^H \mathbf{w}_{s,i} s_{s,i} + \mathbf{n}_s, \quad (1)$$

where $\mathbf{f}_{sU_k}^H = \mathbf{h}_{sU_k}^H + \mathbf{h}_{s,RU_k}^H \mathbf{\Phi}_s(\mathbf{C}) \mathbf{g}_{sR}$ represents the equivalent channel consisting of direct and reflection links; $\mathbf{h}_{sU_k} \in \mathbb{C}^{M\times 1}$, $\mathbf{h}_{s,RU_k} \in \mathbb{C}^{N\times 1}$ and $\mathbf{g}_{sR} \in \mathbb{C}^{M\times N}$ denote the frequency domain channel on frequency f_s from the BSs to the user U_k, from the RIS to U_k, and from BS s to the RIS, respectively. The large-scale fading is given by $C_0(d/d_0)^{-\kappa}$, where κ is the loss exponent caused by the transmission path. The small-scale fading of the channel is modeled as a Rician model with fading parameter λ, which can be expressed as:

$$\mathbf{h} = \sqrt{\frac{\lambda}{1+\lambda}} \mathbf{h}^{\mathrm{LoS}} + \sqrt{\frac{1}{1+\lambda}} \mathbf{h}^{\mathrm{NLoS}}, \quad (2)$$

where the $\mathbf{h}^{\mathrm{LoS}}$ and $\mathbf{h}^{\mathrm{NLoS}} \sim \mathcal{CN}(0, 1)$ denote the Line of Sight and Non-Line of Sight component. It is worth noting that these parameters may be different in different links [18], which will be covered in detail in the simulation setup. $\mathbf{\Phi}_s \triangleq diag(\phi_{s,1}, \phi_{s,2}, \cdots, \phi_{s,N})$ denotes the phase shift matrix at the RIS; n_s is the additive white Gaussian noise (AWGN) at the receiver whose distribution follows $\mathcal{CN}(0, \sigma_s^2)$. Hence, the SINR of the User U_k can be calculated as:

$$\gamma_{s,k} = \frac{\left|\mathbf{f}_{sU_k}^H \mathbf{w}_{s,k}\right|^2}{\sum_{i=1, i\neq k}^{K} \left|\mathbf{f}_{sU_k}^H \mathbf{w}_{s,i}\right|^2 + \sigma_{s,k}^2}. \quad (3)$$

B. Equivalent Circuit Model of RIS

On the basis of the internal structure of the RIS, elements of RIS can be regarded as an impedance model [23], and the Maxwell equation for signal propagation can be reduced to an impedance-based reflection coefficient representation:

$$\phi\left(C_e, R_e, f\right) = \frac{Z_L\left(C_e, R_e, f\right) - Z_0}{Z_L\left(C_e, R_e, f\right) + Z_0}, \quad (4)$$

where the characteristic impedance Z_0 is a fixed value determined by the geometry and material of the transmission path, Z_L is the transmitted load impedance determined by the parameters of the element. Here we use a simplified model that uses fixed inductances and variable capacitor C_e in element e to change Z_L. This model can easily adjust the amplitude and phase of the reflected electromagnetic waves. The load impedance is determined by:

$$Z\left(C_e, R_e, f\right) = \frac{\mathrm{j}2\pi f L_i \left(\mathrm{j}2\pi f L_o + \frac{1}{\mathrm{j}2\pi f C_e} + R_e\right)}{\mathrm{j}2\pi f L_i + \mathrm{j}2\pi f L_o + \frac{1}{\mathrm{j}2\pi f C_e} + R_e}, \quad (5)$$

where L_i, L_o, R_e and f denote the inner layer inductance, the outer layer inductance, resistor, and the carrier frequency, respectively. Noted that the phase of the signal is easier to change compared to the amplitude of the signal by RIS. According to [11], the phase shiftmainly rely on C_e, while other parameters have little influence or difficulty in handling. Therefore, we mainly consider designing the phase shifts by capacitors $\mathbf{C} = \{C_1, C_2, \cdots, C_N\} \in \mathbb{R}^+$ in this paper.

It is evident that the frequency greatly influences the phase shift. Therefore, we hope to present a better downlink performance for users through different responses between frequencies.

C. Problem Fomulation

According to the user's QoS requirements and the overall operating requirements of the system, it is necessary to maximize the sum rate of all users. Although users can receive all frequencies, considering equipment limitations, it will generally select the BS with the highest SINR.

So, we aim to maximize the SR by jointly optimizing the precoding vectors of BSs and the capacitors of RIS elements subject to the power constraint of BSs. Finally, the SR maximization optimization problem can be formulated as:

$$\begin{aligned}\mathcal{P}^0 : &\max_{\mathbf{C},\mathbf{W}} \sum_{k=1}^{K} \max_{s\in\mathcal{B}} \log_2(1+\gamma_{s,k}),\\ &s.t. \sum_{i=k}^{K} |\mathbf{w}_{s,k}|^2 \le P_s, s\in\mathcal{B},\end{aligned} \tag{6}$$

where P_s constrains the maximum power of the BS s. Due to the non-convex of the problem $\mathcal{P}^0$, it is very challenging to get $\mathbf{C}$ and $\mathbf{W}$ directly. We first analyze the maximization problem of the inner layer of $\mathcal{P}^0$ in (6). Evidently, when a user receives a better signal quality from one BS, other BSs can ultimately send no signal to this user. By introducing switch variables $\mathbf{c} = [c_{1,1}, c_{1,2}, \cdots, c_{B,K}]^T$, where:

$$c_{s,k} = \begin{cases} 1, & \text{if } \mathrm{U}_k \text{ choose BS s,}\\ 0, & \text{if } \mathrm{U}_k \text{ choose other BS.}\end{cases} \tag{7}$$

The original problem is equivalent to:

$$\begin{aligned}\mathcal{P}^1 : &\max_{\mathbf{C},\mathbf{W},\mathbf{c}} \sum_{i=1}^{K} c_{s,i}\log_2(1+\gamma_{s,k}),\\ &s.t. \sum_{k=1}^{K} c_{s,k}|\mathbf{w}_{s,k}|^2 \le P_s, s\in\mathcal{B}.\end{aligned} \tag{8}$$

III. SR Maximization Via Preposed Joint Optimization Scheme

In this section, we focus on designing precoding vectors of BSs and capacitors of RIS elements under users choice to maximize the SR of the multi-band heterogeneous network.

The problem $\mathcal{P}^1$ contains non-convex form such as high-dimensional matrix fractions in a sum of logarithms, which cannot be solved by ordinary methods. Fortunately, the multi-dimensional closed-form FP approach based on Lagrangian dual reformulation can effectively reduce the complexity of the problem and decouple the logarithm [18], and a proposition is made as follows.

Proposition 1: By introducing an auxiliary variable $\nu = [\nu_{1,1}, \nu_{1,2}, \cdots, \nu_{B,K}]^T$, the problem $\mathcal{P}^1$ is equivalent to:

$$\begin{aligned}\mathcal{P}^2 : &\max_{\mathbf{C},\mathbf{W},\boldsymbol{\nu},\mathbf{c}} f_{\mathcal{P}^2}(\mathbf{C},\mathbf{W},\boldsymbol{\nu},\mathbf{c}),\\ &s.t. \sum_{k=1}^{K} c_{s,k}|\mathbf{w}_{s,k}|^2 \le P_s, s\in\mathcal{B},\end{aligned} \tag{9}$$

where

$$\begin{aligned}f_{\mathcal{P}^2}(\mathbf{C},\mathbf{W},\boldsymbol{\nu},\mathbf{c}) = &\sum_{s=1}^{B}(\sum_{k=1}^{K} c_{s,k}\log(1+\nu_{s,k})\\ &- c_{s,k}\nu_{s,k} + c_{s,k}(1+\nu_{s,k})\mu_{s,k}),\end{aligned} \tag{10}$$

in which the variable $\mu_{s,k}$ is defined as

$$\mu_{s,k} = \frac{\left|\mathbf{f}_{sU_k}^H \mathbf{w}_{s,k}\right|^2}{\sum_{j=1}^{K}\left|\mathbf{f}_{sU_k}^H \mathbf{w}_{s,j}\right|^2 + \sigma_{s,k}^2}. \tag{11}$$

Therefore, the problem is divided into four sub-problems. Then, we propose an iterative algorithm to optimize the variables $\mathbf{C}$, $\mathbf{W}$, $\boldsymbol{\nu}$ and $\mathbf{c}$ iteratively.

In particular, we firstly assign an initial value to$\mathbf{W}$, $\mathbf{C}$, and $\mathbf{c}$. The optimal solutions to these variables at each step will be introduced in the following three subsections. The solution to $\boldsymbol{\nu}$ is presented in subsection III-A. Then, the solutions to BS precoding vectors $\mathbf{W}$ with auxiliary variable $\boldsymbol{\varpi}$ is described in subsection III-B. Next, the variables $\mathbf{C}$ is transformed into the phase shifts of norm frequency $\boldsymbol{\Phi}_{\mathbf{norm}}$ and an auxiliary variable $\boldsymbol{\chi}$, which is solved in subsection III-C. The solution of switch variables $\mathbf{c}$ is discussed in subsection III-D. Finally, the proposed joint optimization for BS precoding vectors and RIS phase shifts is summarized in Algorithm 1.

A. Fix $\mathbf{C}, \mathbf{W}, \mathbf{c}$ to Find the Optimal $\boldsymbol{\nu}$

As there is no coupling term in $\mathcal{P}^2$ and $\nu_{s,k}$ are all first-order terms, the partial derivatives can be used to solve $\nu_{s,k}$ directly with $\partial f_{\mathcal{P}^2}(\boldsymbol{\nu},\mathbf{W},\mathbf{C})/\partial\nu_{s,k} = 0$. Such that:

$$\nu_{s,k}^{opt} = \frac{\left|\hat{\mathbf{f}}_{sU_k}^H \hat{\mathbf{w}}_{s,k}\right|^2}{\sum_{i=1,i\neq k}^{K}\left|\hat{\mathbf{f}}_{sU_k}^H \hat{\mathbf{w}}_{s,i}\right|^2 + \sigma_{s,k}^2}, \tag{12}$$

where the $\hat{\mathbf{w}}_{s,i}$ and $\hat{\mathbf{f}}_{sU_k}$ are the optimal solutions in the previous round, and the optimal value $\nu_{s,k}^{opt}$ is precisely the SINR $\gamma_{s,k}^{(n-1)}$ obtained in the previous round.

B. Fix $\mathbf{C}, \boldsymbol{\nu}, \mathbf{c}$ to Find the Optimal $\mathbf{W}$

When $\boldsymbol{\Phi}_s(\mathbf{C}), \mathbf{c}, \boldsymbol{\nu}$ are fixed, the precoding vectors $\mathbf{W}$ can be gradually obtained in two steps. Discarding the constant term degenerates the problem into a precoding design. The problem is transformed as:

$$\begin{aligned}\mathcal{P}^{sub-B} : &\max_{\mathbf{W}} f_{\mathcal{P}^{sub-B}}(\mathbf{W}) = \sum_{s=1}^{B}\sum_{k=1}^{K} c_{s,k}(1+\nu_{s,k})\mu_{s,k},\\ &s.t. \sum_{k=1}^{K} c_{s,k}|\mathbf{w}_{s,k}|^2 \le P_s, s\in\mathcal{B}.\end{aligned} \tag{13}$$

Applying the quadratic transform [27] to transform the fractional form in $\mu_{s,i}$ to a convex form, which is reformulated as:

$$\begin{aligned}&f_{\mathcal{P}^{sub-B}}(\mathbf{W},\boldsymbol{\varpi})\\ =&\sum_{s=1}^{B}\sum_{k=1}^{K}(2\sqrt{c_{s,k}(1+\nu_{s,k})}\mathrm{Re}\left\{\varpi_{s,k}\mathbf{f}_{sU_k}^H\mathbf{w}_{s,k}\right\}\\ &-|\varpi_{s,k}|^2(\sum_{j=1}^{K}|\mathbf{f}_{sU_k}^H\mathbf{w}_{s,j}|^2+\sigma_{s,k}^2)),\end{aligned} \tag{14}$$

where $\boldsymbol{\varpi} = [\varpi_{1,1}, \varpi_{1,2}, \cdots, \varpi_{B,K}]^T$ is a set of new auxiliary variables. After the transformation, $\mathcal{P}^{sub-B}$ is similar to the problem $(P1-b)$ in [27], and the alternating optimization (AO) algorithm can solve the problem by optimizing $\boldsymbol{\varpi}$ and $\mathbf{W}$ alternatively. The optimal solution is expressed as:

$$\varpi_{s,k}^{opt} = \frac{\sqrt{c_{s,k}(1+\nu_{s,k})}\mathbf{f}_{sU_k}^H \mathbf{w}_{s,k}}{\sum_{j=1}^{K} |\mathbf{f}_{sU_k}^H \mathbf{w}_{s,j}|^2 + \sigma_{s,k}^2}, \tag{15}$$

which is obtained by the partial derivative. Considering there is no effect between the frequencies, $f_{\mathcal{P}^{sub-B}}$ can be divided into several small targets shown as:

$$\begin{aligned}\hat{\mathcal{P}}_s^{sub-B} : \max_{\mathbf{W}_s} (&2\sqrt{c_{s,k}(1+\nu_{s,k})}\mathrm{Re}\left\{\varpi_{s,k}^H \mathbf{f}_{sU_k}^H \mathbf{W}_s\right\} \\ &- (\mathbf{W}_s^H \sum_{k=1}^{K} (\mathbf{f}_{sU_k}\varpi_{s,k}\varpi_{s,k}^H \mathbf{f}_{sU_k}^H)\mathbf{W}_s \\ &+ \varpi_{s,k}^H \sigma_{s,k}^2 \varpi_{s,k})), \\ s.t. &\mathbf{W}_s^H diag(c_{s,1}, c_{s,2}, , \cdots c_{s,K})\mathbf{W}_s \le P_s, s \in \mathcal{B},\end{aligned} \tag{16}$$

where $\mathbf{W}_s = [\mathbf{w}_{s,1}, \mathbf{w}_{s,2}, \cdots, \mathbf{w}_{s,K}]^T$ is the precoding vector of BS s. Thence the $\sum_{k=1}^{K} (\mathbf{f}_{sU_k}\varpi_{s,k}\varpi_{s,k}^H \mathbf{f}_{sU_k}^H)$ and the constraint $diag(c_{s,1}, c_{s,2}, , \cdots c_{s,K})$ both are positive semidefinite matrices. Moreover, these quadratically constrained quadratic program (QCQP) problems $\hat{\mathcal{P}}_s^{sub-B}$, $s = 1, 2, \cdots, B$ can be solved using convex tools like CVX.

C. Fix $\mathbf{W}, \mathbf{c}, \boldsymbol{\nu}$ to Find the Optimal $\mathbf{C}$

This subsection will propose an algorithm for optimizing $\mathbf{C}$ to manage complex phase shifts in the multi-band heterogeneous networks. By substituting (2) into (1), the relationship between $\phi_{s,e}$ and C_e can be reformulated as:

$$\phi_{s,e} = \frac{a_s C_e + b_s}{c_s C_e + d_s}, \tag{17}$$

where $a_s = (\mathrm{j}2\pi f_s L_i - Z_0)(\mathrm{j}2\pi f_s L_o + R_e - Z_0) - {Z_0}^2$, $b_s = (\mathrm{j}2\pi f_s L_i - Z_0)/\mathrm{j}2\pi f_s$, $c_s = (\mathrm{j}2\pi f_s L_i + Z_0)(\mathrm{j}2\pi f_s L_o + R_e + Z_0) - {Z_0}^2$, and $d_s = (\mathrm{j}2\pi f_s L_i + Z_0)/\mathrm{j}2\pi f_s$.

By analytical derivation, it can be found that C_e appears in both the numerator and the denominator and is highly coupled with frequency. According to [11], C_e generally takes a small value of around 1 pF. The phase is virtually unchanged in an extensive range, but changes sharply in a particular range. The non-linearity characteristics reduce the accuracy of the algorithm and lead to undermined optimization results.

In contrast, the equivalent circuit of RIS is unchanged among all frequency bands. Although the resonant frequencies are variously different, the trends of phase shifts are correlated and can be described as:

$$\begin{aligned}&\phi_{s,e} \\ &= \frac{a_s(b_{norm} - d_{norm}\phi_{norm,e}) + b_s(c_{norm}\phi_{norm,e} - a_{norm})}{c_s(b_{norm} - d_{norm}\phi_{norm,e}) + d_s(c_{norm}\phi_{norm,e} - a_{norm})},\end{aligned} \tag{18}$$

where $\phi_{norm,e} \in \mathbb{C}$, $|\phi_{norm,e}| = 1$ is defined as the phase shift of norm frequency f_{norm} in the element e, and f_{norm} can be chosen prudently among multiple frequencies.

Correspondingly, a_{norm},b_{norm},c_{norm} and d_{norm} represent parameters obtained from (17). Unfortunately, it is still non-convex and hard to solve directly. Inspired by [28], the Taylor expansion can be introduced to approximate the non-convex problems caused by fractions.

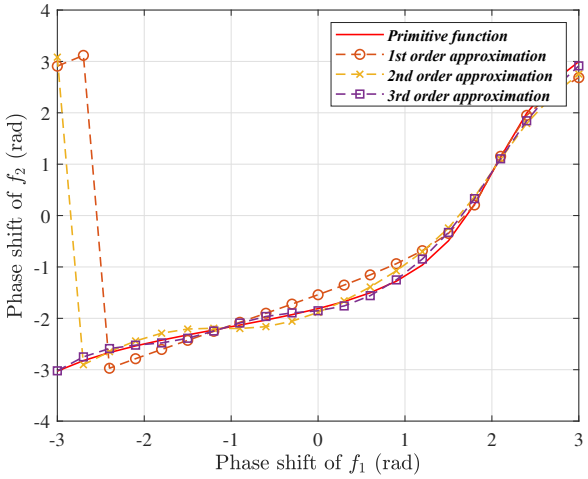

Fig. 2. The approximate result of the proposed scheme.

Lemma 1: $\phi_{s,e}$ can be approximated as:

$$\begin{aligned}\phi_{s,e} &= Q_{f_s}(\phi_{norm,e}), \\ &= \lambda + \alpha \sum_{t=0}^{\infty} (-\beta\phi_{norm,e})^t,\end{aligned} \tag{19}$$

where

$$\begin{aligned}\alpha &= \frac{(a_{norm}d_{norm} - c_{norm}d_{norm})(b_s c_s - a_s d_s)}{(b_{norm}c_s - a_{norm}d_s)(c_{norm}d_s - c_s d_{norm})}, \\ \beta &= \frac{(b_{norm}c_s - a_{norm}d_s)}{(c_{norm}d_s - c_s d_{norm})},\ \lambda = \frac{(b_s c_{norm} - a_s d_{norm})}{(c_{norm}d_s - c_s d_{norm})}.\end{aligned} \tag{20}$$

The convergence domain is $|\beta\phi_{norm,e}| \le 1$. Moreover, the product that likes $\mathbf{Q}^H\mathbf{\Lambda}\mathbf{Q}$ is convex, where $\mathbf{Q}$ is a diagonal matrix and $\mathbf{\Lambda}$ is a positive semidefinite matrix.

Proof: See Appendix A.

Here we have discarded the actual amplitude response. When the resistance is small, the amplitude is basically unchanged, which makes the approximation reasonable. Although the calculation of the coefficients becomes more complicated, once the system frequency is determined, it does not need to be calculated again. Fig.2 demonstrates the original relationship and the result of three different order approximation using complex Taylor expansion.

While the result have deviation when phase shift of f_1 is close to $\pm\pi$, the phase shift of f_2 is close to $\pm\pi$ too, which has little effect on results. It is easy to obtain an acceptable approximation by removing some high-order terms. Therefore, the original question can be reformulated into:

$$\begin{aligned}\mathcal{P}^{sub-C} : &\max_{\mathbf{\Phi_{norm}}} \sum_{s=1}^{B}\sum_{k=1}^{K} c_{s,k}(1+\nu_{s,k}) g_{s,k}(\mathbf{\Phi}_{norm}, \mathbf{W}^*), \\ &s.t.\ \phi_{norm,e} \in \mathbb{C}, |\phi_{norm,e}| = 1\ \forall e \in \mathcal{N},\end{aligned} \tag{21}$$

where

$$g_{s,k}(\mathbf{\Phi}_{norm}, \mathbf{W}^*) = \frac{\left|\left(\mathbf{h}_{sU_k}^H + \mathbf{h}_{s,RU_k}^H \mathbf{Q}_{f_s}(\Phi_{norm})\mathbf{g}_{sR}\right)\mathbf{w}_{s,k}^*\right|^2}{\sum_{j=1}^{K}\left|\left(\mathbf{h}_{sU_k}^H + \mathbf{h}_{s,RU_k}^H \mathbf{Q}_{f_s}(\Phi_{norm})\mathbf{g}_{sR}\right)\mathbf{w}_{s,j}^*\right|^2 + \sigma_{s,i}^2}. \tag{22}$$

Therefore, the original problem which optimizes the capacitors of RIS elements $\mathbf{C}$, changes into the problem aiming at the phase shifts of the norm frequency $\mathbf{\Phi}_{norm}$.

However, it is still complicated to solve the high dimensionality caused by a large number of RIS elements and the fractional form. Specifically, unlike solving the precoding vectors, the phase shifts involve the inversion and multiplication of the matrix, which cannot be directly simplified into the form that can be solved. We exploit the multi-dimensional complex quadratic transform (MCQT) [29] to solve the coupling problem of high-dimensional matrices. By extending FP to matrix form, MCQT provides the ability to solve such problems. For simplicity, $\mathbf{\Theta_{s,k,j}}$ is denoted as:

$$\mathbf{\Theta}_{s,k,j} = (\mathbf{h}_{sU_k}^H + \mathbf{h}_{s,RU_k}^H \mathbf{Q}_s(\mathbf{\Phi}_{norm})g_{sR})\mathbf{w}_{s,j}^*, \tag{23}$$

and $g_{s,k}$ in (22) can be rewritten as:

$$g_{s,k}(\mathbf{\Phi}_{norm}, \mathbf{W}^*) = \mathbf{\Theta}_{s,k,k}^H(\sum_{j=1}^{K}\mathbf{\Theta}_{s,k,j}\mathbf{\Theta}_{s,k,j}^H)^{-1}\mathbf{\Theta}_{s,k,k}. \tag{24}$$

Then we obtain the Proposition 2 to reformulate the non-convex problem:

Proposition 2: By introducing auxiliary variables $\boldsymbol{\chi} = [\chi_{1,1}, \chi_{1,2}, \cdots, \chi_{B,K}]^T$, the problem is transformed $\mathcal{P}^{sub-C}$ via MCQT method [29] as:

$$\begin{aligned} &\max_{\mathbf{\Phi}_{norm}, \boldsymbol{\chi}} f_{\mathcal{P}^{sub-C}}(\mathbf{\Phi}_{norm}), \\ &s.t. \phi_{norm,e} \in \mathbb{C}, |\phi_{norm,e}| = 1, \forall e \in \mathcal{N}. \end{aligned} \tag{25}$$

where

$$\begin{aligned} f_{\mathcal{P}^{sub-C}}(\mathbf{\Phi}_{norm}) &= \sum_{s=1}^{B}\sum_{k=1}^{K} 2\sqrt{c_{s,k}(1+\nu_{s,k})}\mathrm{Re}(\chi_{s,k}^H \mathbf{\Theta}_{s,k,k}) \\ &\quad - \chi_{s,k}^H(\sum_{j=1}^{K}\mathbf{\Theta}_{s,k,j}\mathbf{\Theta}_{s,k,j}^H)\chi_{s,k}. \end{aligned} \tag{26}$$

Then the $\mathbf{\Phi}_{norm}$ can be updated in two steps:

1) Fix $\mathbf{\Phi}_{norm}$ to find optimal $\boldsymbol{\chi}$: For given $\mathbf{\Phi}_{norm}$, the optimal value of $\chi_{s,k}$ is reduced to a quadratic function. By directly taking the partial derivative as $\partial f_{\mathcal{P}^{sub-C}}/\partial\chi_{s,k} = 0$, we obtain the optimal value as follows.

$$\chi_{s,k}^{opt} = \sqrt{c_{s,k}(1+\nu_{s,k})}\mathbf{\Theta}_{s,k,k}(\sum_{j=1}^{K}\mathbf{\Theta}_{s,k,j}\mathbf{\Theta}_{s,k,j}^H)^{-1}. \tag{27}$$

2) Fix $\boldsymbol{\chi}$ to find optimal $\mathbf{\Phi}_{norm}$: Note that, the last term of (26) can be expressed by the sum of quadratic form like: $\sum_{j=1}^{K}\chi_{s,k}^H\mathbf{\Theta}_{s,k,j}(\chi_{s,k}^H\mathbf{\Theta}_{s,k,j})^H$ Thus, substituting (23) we can obtain the relationship as follow:

$$\begin{aligned} &\chi_{s,k}^H\mathbf{\Theta}_{s,k,j} \\ &\overset{(a)}{=} \chi_{s,k}^H\mathbf{h}_{s,RU_k}^H\mathbf{w}_{s,j} + \chi_{s,k}^H\mathbf{h}_{s,RU_k}^H\mathbf{Q}_s(\mathbf{\Phi}_{norm})\mathbf{g}_{sR}\mathbf{w}_{s,j} \\ &\overset{(b)}{=} \chi_{s,k}^H\mathbf{h}_{s,RU_k}^H\mathbf{w}_{s,j} + \mathbf{Q}_s(\boldsymbol{\theta})^H diag(\chi_{s,k}^H\mathbf{h}_{s,RU_k}^H)\mathbf{g}_{sR}\mathbf{w}_{s,j}, \end{aligned} \tag{28}$$

where (a) is obtained by substituting (23) into $\mathbf{\Theta_{s,k,j}}$, and (b) is derived by changing the form of the multiplication of vector and matrix [30]. $\mathbf{Q}_s(\boldsymbol{\theta})^H$ is the calculated phase shift vector and $\boldsymbol{\theta} = [\theta_1, \theta_2, \cdots, \theta_N]^T$, where $\theta_n = \Phi_{norm}(n,n)\forall n \in N$. By defining $\alpha_{s,k,j} = \chi_{s,k}^H\mathbf{h}_{s,RU_k}^H\mathbf{w}_{s,j}$ and $\boldsymbol{\beta}_{s,k,j} = diag(\chi_{s,k}^H\mathbf{h}_{s,RU_k}^H)\mathbf{g}_{sR}\mathbf{w}_{s,j}$, the $f_{q_3}(\mathbf{\Phi}_{norm})$ can be simplified as:

$$\begin{aligned} &f_{\mathcal{P}^{sub-C}}(\mathbf{\Phi}_{norm}) \\ &\overset{(a)}{=} -\sum_{s=1}^{B}\sum_{k=1}^{K}\sum_{j=1}^{K}\mathbf{Q}_s(\theta)^H\boldsymbol{\beta}_{s,k,j}\boldsymbol{\beta}_{s,k,j}^H\mathbf{Q}_s(\theta) \\ &\quad + \sum_{s=1}^{B}\sum_{k=1}^{K}\mathrm{Re}(2\sqrt{c_{s,k}(1+\nu_{s,k})}\mathbf{Q}_s(\theta)^H\boldsymbol{\beta}_{s,k,k} \\ &\quad - \sum_{j=1}^{K}2\mathbf{Q}_s(\theta)^H\boldsymbol{\beta}_{s,k,j}\alpha_{s,k,j}^H) \\ &\quad + \sum_{s=1}^{B}\sum_{k=1}^{K}\mathrm{Re}(2\sqrt{c_{s,k}(1+\nu_{s,k})}\alpha_{s,k,j} - \sum_{j=1}^{K}|\alpha_{s,k,j}|^2), \end{aligned} \tag{29}$$

where (a) is obtained by substituting $\alpha_{s,k,j}$ and $\boldsymbol{\beta}_{s,k,j}$ into $f_{\mathcal{P}^{sub-C}}(\mathbf{\Phi}_{norm})$. Let $\mathbf{\Lambda}_s = \sum_{k=1}^{K}\sum_{j=1}^{K}\boldsymbol{\beta}_{s,k,j}\boldsymbol{\beta}_{s,k,j}^H$, and $\mathbf{\Gamma}_s = \sum_{k=1}^{K}2\sqrt{c_{s,k}(1+\nu_{s,k})}\boldsymbol{\beta}_{s,k,k} - \sum_{j=1}^{K}2\boldsymbol{\beta}_{s,k,j}\alpha_{s,k,j}^H$. After ignoring the last constant term, the problem finally turns into:

$$\begin{aligned} \hat{\mathcal{P}}^{sub-C} : &\max_{\theta} -\sum_{s=1}^{B}\mathbf{Q}_s(\theta)^H\mathbf{\Lambda}_s\mathbf{Q}_s(\theta) + 2\mathrm{Re}\{\mathbf{Q}_s(\theta)^H\mathbf{\Gamma}_s\}, \\ &s.t. \theta_n \in \mathbb{C}, |\theta_n| = 1. \end{aligned} \tag{30}$$

So far, the matrix $\mathbf{\Lambda}_s$ and constraint are positive semidefinite. According to Lemma 1, the problem $\hat{\mathcal{P}}^{sub-C}$ can be solved by ADMM using convex optimization tools like CVX.

D. Fix $\mathbf{\Phi}_{norm}, \mathbf{W}, \boldsymbol{\nu}$ to Find the Optimal $\mathbf{c}$

After obtaining the current optimal result, users will automatically access to the corresponding BS. Hence, the problem is reformulated as follows:

$$\mathcal{P}^{sub-D} : \max_{\mathbf{c}} f_{\mathcal{P}^{sub-D}}(\mathbf{c}) \tag{31}$$

where

$$\begin{aligned} f_{\mathcal{P}^{sub-D}}(\mathbf{c}) = \sum_{s=1}^{B}(\sum_{k=1}^{K} &c_{s,k}\log(1+\nu_{s,k}^{opt}) \\ &- c_{s,k}\nu_{s,k}^{opt} + c_{s,k}(1+\nu_{s,k}^{opt})\mu_{s,k}^{opt}). \end{aligned} \tag{32}$$

However, random selection on $c_{s,i}$ usually fail to achieve optimal results. The greedy traversal search can be used to obtain the optimal solution, but the complexity will be unacceptable when there are more users. The computation complexity will multiply B^K, which will lead to a poor adaptable usage in specific scenarios.

Therefore, we propose a fast search algorithm based on GA [31], reducing the computational complexity and improving the convergence speed. GA is an adaptive probabilistic optimization technique based on biological and evolutionary mechanisms. The algorithm obtains an approximation to the global optimum through crossover and mutation between populations. GAs prove their potential in finding exact or near-optimal solutions in a series of complex system optimization calculations for the wireless network [32].

For this problem, we initialize the first population $P_1 = [p_i], i = 1, 2, \cdots, I_1$ with size I_1, in which each individual $p_i = [c_k], k = 1, 2, \cdots, K$ is a set of BS selections by users. Individuals are encoded in binary, and c_k represents the user's selection of BS. For example, if the s-th BS is selected, it is recorded as 2^{s-1}.

Afterwards, the fitness function $F(p_i)$ takes the optimal result of $f_{\mathcal{P}^{sub-D}}(\mathbf{c})$, that is, the maximum SR obtained through iterative optimization in the current situation. Subsequently, the evolution of the next population is carried out through the following operations:

Survival selection operation: Individuals with high fitness have a higher chance of surviving. According to the roulette wheel [31], we present the survival probability $S(p_k)$ of p_k as:

$$S(p_k) = \frac{F(p_k)}{\sum\limits_{i \in I} F(p_i)}. \tag{33}$$

Crossover and mutation operation: The crossover operator $X(p_i, p_j)$ randomly selects two individuals p_i and p_j as parents.Since the positions of genes represent different users, we adopt a multi-point average crossover method. The two parents swap the elements with a certain probability and derive two new member of next generation. The mutation operator $M(p_l)$ randomly selects as individual p_l, and changes user choices with some specific probability. The user with lowest SINR is choosed and changes its choice by randomly changing the bit in the c_l. The subsequent population is gradually generated through the above two operators until the quantity requirements are met.

Finally, the generations are obtained through the above manner until the termination condition (i.e., the number of iterations T) has reached the set value. Compared with the greedy traversal search, GA can effectively reduce the complexity and obtain an acceptable global optimal solution by reasonably setting the population size I_g and the number of iterations T.

The overall algorithm is summarized in **Algorithm 1**. To demonstrate the effectiveness of the proposed algorithm, we test the achievable performance in 4 BSs and 6 users. The population size is set between 10 and 20 times the number of BSs (i.e., 80) and the number of iterations is set as T = 100 in this case. As shown in Fig.3, the proposed algorithm can obtain similar results to the optimal result of traversal algorithm in an effective time.

Algorithm 1 Proposed joint Optimization algorithm for solving $\mathcal{P}^1$

Input: The channels $\mathbf{h}_{sU_k}$, $\mathbf{h}_{s,RU_k}$ and $\mathbf{g}_{sR}$ with $\forall k = 1 \cdots K, \forall s = 1 \cdots B$

Output: Optimized SR with optimal BS precoding vectors $\mathbf{W}$, RIS phase shifts of norm frequency $\boldsymbol{\theta}$ and optimal BS choices $\mathbf{c}$

```
Initialize W, θ and c and generate initial population P_t, t = 1
while t ≤ T, do
    while no convergence of R_sum, do
        Update ν by (12)
        Update ϖ by (15)
        for s = 1 to B do
            Update W_s by solving (16)
        end for
        Update χ by (27)
        Update θ by solving (30)
    end while
    Calulate fitness function in (33)
    Perform Crossover X(p_i, p_j) and mutation M(p_l)
    Recieve the next generation P_{t+1}
end while
return W, θ and c;
```

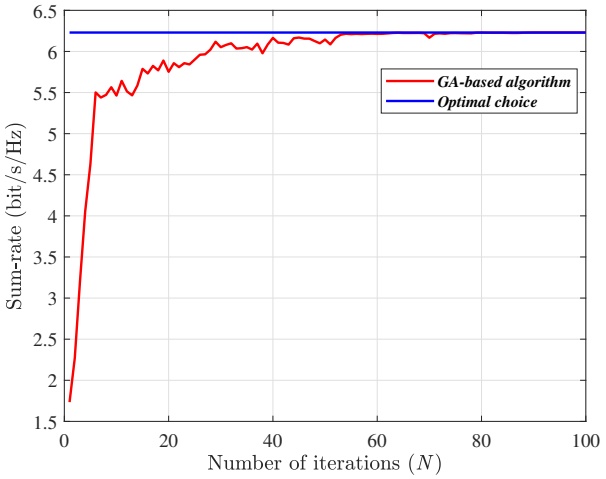

Fig. 3. The number of iterations vs. SR.

Complexity Analysis: According to [29], the complexity of the whole problem can be regarded as a sum of the complexity of sub-problems. The main complexity comes from the sub-problem B and C, and the ADMM method needs to calculate the inverse of a high-dimension matrix in solving QCQP problems. Therefore, the main computational complexity can be abstracted as $\mathcal{O}(I_b B^3 M^3 K^3)$ in solving $\hat{\mathcal{P}}^{sub-B}$ and $\mathcal{O}(I_c N^3)$ in solving $\hat{\mathcal{P}}^{sub-C}$, where I_b and I_c are the iteration number. Finally, the computational complexity of the entire algorithm can be expressed as $\mathcal{O}(I_g \times T \times I_n(I_b B^3 M^3 K^3 + I_c N^3))$, where I_n is the iterations number for convergence.

IV. Simulation Results

For simplicity but without loss of generalization, we establish a system with two BSs (denoted as BS A and BS B), serving four users as the experimental environment. The frequency bands of the BSs are 2.3 GHz and 2.5 GHz, respectively, and the user can select which BS to access to. There is a RIS in the system, and is modeled as the practical model including phase and amplitude response and the basic parameters of each unit are: $L_i = 2.5$ nH, $L_o = 0.7$ nH and $R_e = 0.01\ \Omega$. The wireless transmission medium is set as $Z_0 = 377\ \Omega$ in the air. Unless otherwise specified, we set locations of BSs as $(80, -50)$ and $(90, -50)$, users as $(20, 0)$, $(60, 0)$, $(100, 0)$ and $(140, 0)$, and the RIS as $(60, 10)$. The number of BS's antennas is 4, and the maximum transmit power is 1mW. The number of user's antennas is 1, the number of RIS reflection units is 80, and the noise power is -80dbm.

As for the channel model, the large-scale fading of the BS-RIS link is set as $\kappa_{sU_k} = 2.5$, and the RIS-User and BS-User links are set as $\kappa_{sR} = 2.8$ and $\kappa_{s,RU_k} = 3.5$, respectively, which are the same as[4]. For the small-scale fading, the LoS component of the BS-RIS link is generally considered to be larger and let $\lambda_{sR} = 10$, while the BS-User and RIS-User mainly depend on the NLoS path and are assumed as $\lambda_{sU_k} = \lambda_{s,RU_k} = 0.1$.

The schemes we compared are as follows:

1) Baselines: The random phase shift scheme (denoted as the RND scheme) and no RIS scheme (denoted as the no_RIS scheme). The phase shifts of RIS change randomly between time slots in the RND scheme. While the BSs optimize their precoding vectors without RIS in the no_RIS scheme. Users will select the BS according to the signal power.

2) The joint precoding scheme method only considers BS A (denoted as the OCA scheme): in the network, BS A uses the joint precoding method proposed in [27] to optimize its precoding vector and phase shifts. In contrast, BS B designs the precoding vector according to the CSI obtained in the training phase. It will be affected by the RIS controlled by BS A in the subsequent transmission stage.

3) Proposed scheme with fixed users (denoted as the FU scheme): the joint precoding framework in [25], where users can only access to the specific BS, and BSs optimize the SR of their own users. Unless otherwise specified, we generally assume that users 1 and 3 access to BS A and the rest access to BS B.

A. The Number of RIS Elements vs. SR

Fig. 4 presents the number of elements at RIS against SR. We can observe that with the increase of N, the performance of the proposed scheme, the OCA scheme and the FU scheme improved, while the no_RIS and RND schemes have subtle changes. Moreover, the performance improvement of the proposed scheme is conspicuous. The FU scheme has lower SR because the user's choices are not considered to achieve the optimal choice. In addition, we find that the OCA scheme will indeed have a more significant impact on the SR, and the performance of the system is worse than no_RIS scheme when the number of RIS is small. This is because the improvement

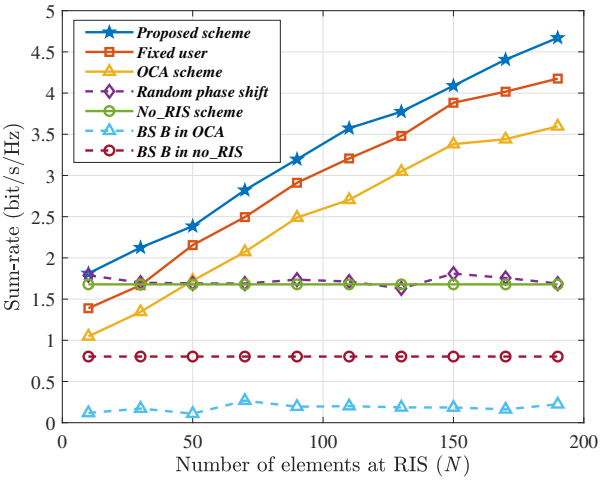

Fig. 4. The number of RIS elements vs. SR.

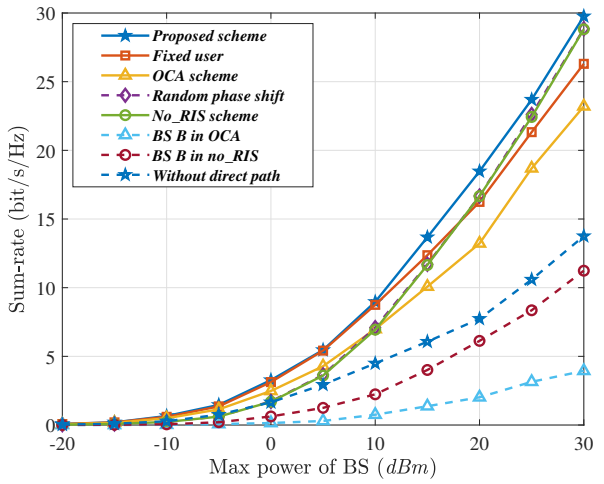

Fig. 5. The max power constraint vs. SR.

contributed by RIS to BS A cannot make up for the loss to BS B. Three lines at the bottom of the figure compare the rate of BS B among the proposed scheme, no_RIS and OCA. With the increase of N, the rate of BS B does not change significantly as it is in the OCA scheme, and is lower than no_RIS, which is predictable. We explain this phenomenon in detail as follows. Due to the channel's independence, the reflet link is actually equivalent to a random phase shift obeying a complex Gaussian distribution, according to the central limit theorem. The unintended channel overlay makes the designed precoding no longer suitable for the actual channel, makes the beam no longer aim at users, and even increases the interference. Therefore, the loss of BS in OCA results in a lower SR than the RND scheme and the no_RIS scheme.

B. The Max Power Constraint vs. SR

Fig. 5 shows the relationship between the max power of BS and SR. The SR of each scheme increases as the power rises, and the proposed scheme has the highest SR. When the power

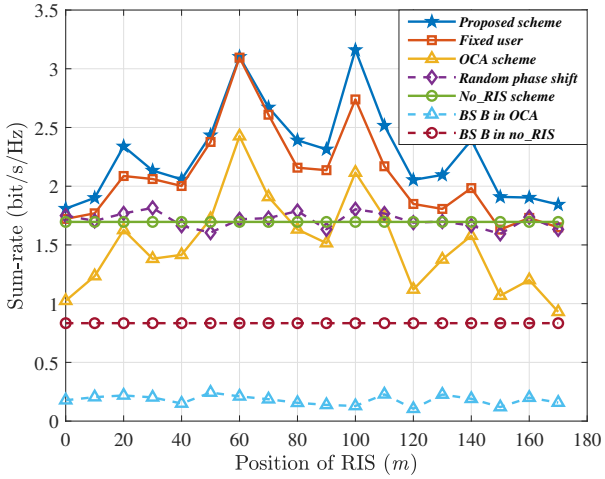

Fig. 6. The position of RIS vs. SR.

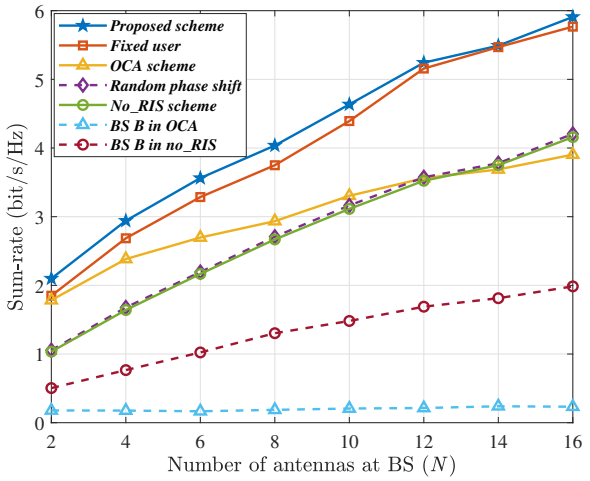

Fig. 7. The number of antennas vs. SR.

is very small, the RIS's reflected signal is extremely low due to the path loss, so the actual SR of various schemes is almost the same. When the transmit power of BSs is extremely large, since the actual channel of the direct link is better, the designed precoding vector is more inclined to allocate power to the direct link rather than the reflect link, making the proposed scheme almost the same as no_RIS. To this end, we also performed a simulation without the direct path, and it can be seen that the growth rate is very low, which also proves this trend.

In the FU scheme, when the power is further increased, the power of serving users tends to be saturated so that the SR may be limited. In the OCA scheme, it can be seen that the increase rate of BS B is very slow compared with no_RIS, resulting in a consistently lower SR.

C. The Position of RIS vs. SR

We present the SR with different positions of RIS in Fig. 6. Regardless the RIS moving from 0 to 180m on the x axis, the proposed scheme has the highest SR. When the RIS is close to users, there are spikes of SR, such as 24, 60, 100, and 140. This phenomenon implies that the RIS should be deployed closer to the user. In the FU scheme, SR is degraded compared with the proposed scheme, unless user choices are the same as the optimal choices (which will happen in 40–80 meters). The OCA scheme is lower than the no-RIS and RND schemes, except in some locations where RIS is very close to the user. Finally, as it can be seen from the two lines below, the position of RIS also has no significant effect on the BS B in the OCA scheme.

D. The Number of Antennas vs. SR

Fig. 7 shows the relation between SR and the number of antennas. The SR rises with the increase of antennas, and the proposed scheme outperforms the other schemes. When the number of antennas is large, the SR of the proposed scheme is closer to that of the FU scheme. That is because the energy can be more focused on the target users, which will reduce the power requirements. The users of BSB under OCA scheme hardly increases with the number of antennas. This is because the BSB has no knowledge of the channel changes by RIS, which makes its precoding completely invalid and cannot benefit from multi-antenna diversity. Although the number of antennas increases, the precoding of BSB in OCA is entirely invalid, which does not increase the actual SR. Therefore, the SR is even worse than the no_RIS scheme when the number of antennas is large. This further illustrates that deploying RIS recklessly will have a great impact on other systems.

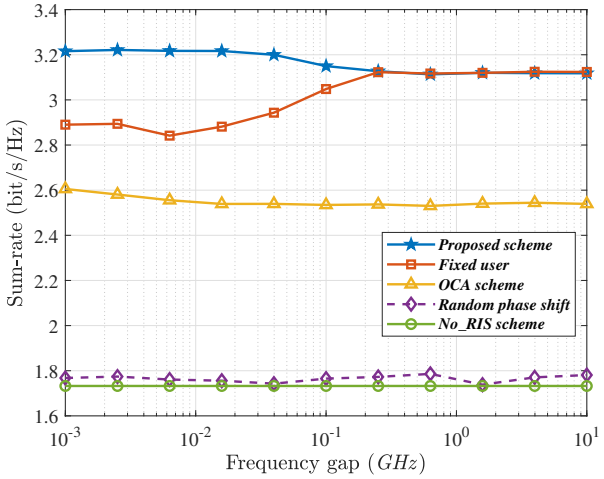

Fig. 8. The frequency gap vs. SR.

E. The Frequency Gap vs. SR

Fig. 8 shows the adaptation of the algorithm for different frequency gap between two frequency bands. The proposed scheme has the highest SR at various frequency gaps. Due to the model accuracy, the FU scheme has less SR compared with the proposed scheme in a small frequency gap. When the frequency gap is enormous, since most of the phase shifts

are approximately 0 or 2π, the actual SR is degraded in the proposed scheme. At the same time, the SR of the OCA scheme is lower than the above two schemes and has similar trends with the proposed scheme.

V. Conclusion

In this paper, we propose RIS-assisted multi-band heterogeneous networks where BSs serve multiple users over multiple frequency bands. The RIS utilizes its frequency-related responses to enhance the overall performance of the network. In this scenario, by jointly designing the precoding vector of each BS and the phase shifts of the RIS, the SR is maximized using an iterative optimization algorithm. The simulation results show that the proposed scheme can effectively improve the overall performance of the multi-band heterogeneous networks. We further investigate the effects of different RIS elements numbers, deployment locations, and frequency gaps to provide guidance for RIS deployment. At the same time, the results verify that unplanned RIS deployment has no benefit to the network but will destroy the stability of the existing system. Possible directions for future works include more complex scenarios such as cell-free networks, and more practical models such as discrete phase-shift.

Appendix A
Proof of Lemma 1

By expanding with Taylor expansion, (18) can be converted into:

$$\begin{aligned}&\phi_{s,e}\\&=\frac{a_s(b_{norm}-d_{norm}\phi_{norm,e})+b_s(c_{norm}\phi_{norm,e}-a_{norm})}{c_s(b_{norm}-d_{norm}\phi_{norm,e})+d_s(c_{norm}\phi_{norm,e}-a_{norm})}\\&=\lambda+\alpha(\frac{1}{1+(\beta\phi_{norm,e})}).\end{aligned} \tag{34}$$

Because the $\phi_{norm,e}\in\mathbb{C}$, the premise of Taylor expansion of complex variables is that the power series can be analytic in the circle of convergence. While in (34), the region of convergence is $|\beta\phi_{norm,e}|\leq 1$. Unfortunately, we find that $|\beta|=1$ when $|f_{norm}-f_s|\to\infty$, and $|\beta|>1$ when the frequency gap is small. That means the $\phi_{norm,e}$ could not converge to the unit circle. However, it is worth pointing out that since we mainly consider the change of phase here, which β only changes the phase of $\phi_{norm,e}$. That means that although the absolute value of the expansion may not converge when $|\phi_{norm,e}|=1$, the phase of the expansion is always converged no matter what value β takes.

Furthermore, the complex function which likes $\mathbf{Q}^H\mathbf{\Lambda}\mathbf{Q}$ is convex, where the diagonal matrix $\mathbf{Q}$ calculating by (19), and the positive semidefinite matrix $\mathbf{\Lambda}$. Because the Hessian matrix of it is a positive semidefinite matrix in 0-order term, 1-order term and the remaining high-order terms, which can be expressed as:

$$\begin{bmatrix}\left(\theta_1^H\theta_1\right)^{t-2}\Lambda_{s,1} & 0 & \cdots & 0\\ 0 & \left(\theta_2^H\theta_2\right)^{t-2}\Lambda_{s,2} & 0 & 0\\ \vdots & 0 & \ddots & \vdots\\ 0 & 0 & \cdots & \left(\theta_n^H\theta_n\right)^{t-2}\Lambda_{s,n}\end{bmatrix}. \tag{35}$$

Thence, it can be solved by convex optimization methods.

References

[1] Z. Zhang, *et al*., "6g wireless networks: Vision, requirements, architecture, and key technologies," *IEEE Veh. Technol. Mag.*, vol. 14, no. 3, pp. 28–41, 2019.

[2] H. Li, R. Liu, M. Liy, Q. Liu, and X. Li, "IRS-enhanced wideband MU-MISO-OFDM communication systems," in *Proc. IEEE WCNC*, 2020.

[3] F. Kilinc, I. Yildirim, and E. Basar, "Physical channel modeling for RIS-empowered wireless networks in sub-6 GHz bands : (Invited Paper)," in *IEEE Proc. Asilomar Conf. Signals, Syst. Comput.*, 2021.

[4] J. Xu and Y. Liu, "A novel physics-based channel model for reconfigurable intelligent surface-assisted multi-user communication systems," *IEEE Trans. Wireless Commun.*, vol. 21, no. 2, pp. 1183–1196, 2022.

[5] K. Liu and Z. Zhang, "On the energy-efficiency fairness of reconfigurable intelligent surface-aided cell-free network," in *Proc. IEEE VTC*, 2021.

[6] Q. Zhu, H. Li, R. Liu, M. Li, and Q. Liu, "Hybrid beamforming and passive reflection design for RIS-assisted mmWave MIMO systems," in *Proc. IEEE ICC*, 2021.

[7] Z. Tang, T. Hou, Y. Liu, J. Zhang, and C. Zhong, "A novel design of RIS for enhancing the physical layer security for RIS-Aided NOMA Networks," *IEEE Wireless Commun. Lett.*, vol. 10, no. 11, pp. 2398–2401, 2021.

[8] Y. Chen, *et al*., "Reconfigurable intelligent surface assisted device-to-device communications," *IEEE Trans. Wireless Commun.*, vol. 20, no. 5, pp. 2792–2804, 2021.

[9] Z. Chu, *et al*., "Resource allocation for IRS sssisted wireless powered FDMA IoT networks," *IEEE Trans. Wireless Commun.*, vol. 18, no. 2, pp. 1447–1461, 2019.

[10] E. Bjornson, *et al*., "Reconfigurable intelligent surfaces: A signal processing perspective with wireless applications," *IEEE Signal Process. Mag.*, vol. 39, no. 2, pp. 135–158, 2022.

[11] Y. C. Liang, *et al*., "Reconfigurable intelligent surfaces for smart wireless environments: Channel estimation, system design and applications in 6G networks," *Sci. China Inf. Sci.*, vol. 64, no. 10, p. 200301, 2021.

[12] O. Ozdogan, E. Bjornson, and E. G. Larsson, "Intelligent reflecting surfaces: Physics, propagation, and pathloss modeling," *IEEE Wireless Commun. Lett.*, vol. 9, no. 5, pp. 581–585, 2020.

[13] Y. Huo, X. Dong, W. Xu, and M. Yuen, "Cellular and WiFi co-design for 5G user equipment," in *IEEE 5G World Forum*, 2018.

[14] W. Saad, M. Bennis, and M. Chen, "A vision of 6g wireless systems: Applications, trends, technologies, and open research problems," *IEEE Network*, vol. 34, no. 3, pp. 134–142, 2020.

[15] Y. Yang, S. Zhang, and R. Zhang, "IRS-enhanced OFDM: Power allocation and passive array optimization," in *Proc. IEEE GLOBECOM*, 2019.

[16] Y. Yang, B. Zheng, S. Zhang, and R. Zhang, "Intelligent reflecting surface meets OFDM: Protocol design and rate maximization," *IEEE Trans. Commun.*, vol. 68, no. 7, pp. 4522–4535, 2020.

[17] C. Xu, *et al*., "Reconfigurable intelligent surface assisted multi-carrier wireless systems for doubly selective high-mobility ricean channels," *IEEE Trans. Veh. Technol.*, vol. 71, no. 4, pp. 4023–4041, 2022.

[18] Z. Zhang and L. Dai, "A joint precoding framework for wideband reconfigurable intelligent surface-aided cell-free network," *IEEE Trans. Signal Process.*, vol. 69, pp. 4085–4101, 2021.

[19] J. Li, T. A. Denidni, and Q. Zeng, "A dual-band reconfigurable radiation pattern antenna based on active frequency selective surfaces," in *Proc. IEEE APSURSI*, 2016.

[20] Y. Gao and X. Chen, "Novel electromagnetic energy selective surface with frequency selection," in *Proc. IEEE CSRSWTC*, 2020.

[21] C. Liaskos, *et al*., "A new wireless communication paradigm through software-controlled metasurfaces," *IEEE Commun. Mag.*, vol. 56, no. 9, pp. 162–169, 2018.

[22] F. Liu, *et al*., "Intelligent metasurfaces with continuously tunable local surface impedance for multiple reconfigurable functions," *Phys. Rev. Appl.*, vol. 11, no. 4, p. 1, 2019.
[23] S. Abeywickrama, R. Zhang, Q. Wu, and C. Yuen, "Intelligent reflecting surface: Practical phase shift model and beamforming optimization," *IEEE Trans. Commun.*, vol. 68, no. 9, pp. 5849–5863, 2020.
[24] F. Costa and M. Borgese, "Electromagnetic model of reflective intelligent surfaces," *IEEE Open J. Commun. Soc.*, vol. 2, pp. 1577–1589, 2021.
[25] W. Cai, R. Liu, Y. Liu, M. Li, and Q. Liu, "Intelligent reflecting surface assisted multi-cell multi-band wireless networks," in *Proc. IEEE WCNC*, 2021.
[26] H. Li, *et al*., "Intelligent reflecting surface enhanced wideband MIMO-OFDM communications: From practical model to reflection optimization," *IEEE Trans. Commun.*, vol. 69, no. 7, pp. 4807–4820, 2021.
[27] J. Hu, Y.-C. Liang, and Y. Pei, "Intelligent reflecting surface enhanced multi-user MISO symbiotic radio systems," in *Proc. IEEE ICC*, 2021.
[28] B. Fang, Z. Qian, W. Zhong, and W. Shao, "Iterative precoding for MIMO wiretap channels using successive convex approximation," in *Proc. IEEE APCAP*, 2015.
[29] K. Shen and W. Yu, "Fractional programming for communication systems - part I: Power control and beamforming," *IEEE Trans. Signal Process.*, vol. 66, no. 10, pp. 2616–2630, 2018.
[30] X. Guan, Q. Wu, and R. Zhang, "Intelligent reflecting surface assisted secrecy communication: Is artificial noise helpful or not?" *IEEE Wireless Commun. Lett.*, vol. 9, no. 6, pp. 778–782, 2020.
[31] C. W. Ahn, "Practical genetic algorithms," in *Studies in Computational Intelligence*, Berlin/Heidelberg: Springer-Verlag, 2006, vol. 18, pp. 7–22. [Online]. Available: http://link.springer.com/10.1007/11543138_2
[32] K. P. Ferentinos and T. A. Tsiligiridis, "Adaptive design optimization of wireless sensor networks using genetic algorithms," *Comput. Networks*, vol. 51, no. 4, pp. 1031–1051, 2007.

Wenyu Jiang received the B.E. degree in Electronic and Telecommunication Engineering from Information Engineering University, Zhengzhou China in 2020, where he is currently working toward the Ph.D. degree in Information Engineering. His research interests include reconfigurable intelligent surface and anti-jamming technology. He was the Recipient of the Excellent Thesis Award of Information Engineering University in 2020.

Kaizhi Huang received the B.E. degree in Digital Communication and the M.S. degree in Communication and Information System from the National Digital Switching System Engineering and Technological Research Center (NDSC), in 1995 and 1998, respectively, and the Ph.D. degree in communication and information system from Tsinghua University, Beijing, China, in 2003. She has been a Faculty Member of NDSC, since 1998, where she is currently a Professor and the Director of the Laboratory of Mobile Communication Networks. Her research interests include wireless network security and signal processing.

Yajun Chen received the B.E. degree from UESTC University, and the M.S. and Ph.D. degrees from the National Digital Switching System Engineering and Technological R&D Center (NDSC), Zhengzhou, China. He has been a Faculty Member of NDSC, since 2017. His research interests include physical layer security, wireless location, and resource management in 5G networks.

Xiaoli Sun was born in 1992. She received the Ph.D. degree from Army Engineering University of PLA. She is currently a Lecturer of PLA Strategic Support Force Information Engineering University, Zhengzhou, China. Her research interests include wireless communications and physical layer security.

Jie Yang received the M.S. degree in Communication Engineering from the College of Communications Engineering, PLA University of Science and Technology, Nanjing, China, in 2017. He is currently pursuing the Ph.D. degree with the National Digital Switching System Engineering and Technological Research and Developing Center, Zhengzhou, China. His major research interests include wireless communication security and secret key generation.

Kai Zhao obtained his bachelor's degree in Electronic Engineering from Nanjing University of Posts and Telecommunications in 2005 and the intermediate title of Software Designer issued by the Ministry of Industry and Information Technology and the Ministry of Personnel in 2004. At present, he is a Senior System Engineer in Purple Mountain Laboratories. His research interests include wireless network security and data transmission.